

REPORT DOCUMENTATION PAGE

*Form Approved
OMB No. 0704-0188*

The public reporting burden for this collection of information is estimated to average 1 hour per response, including the time for reviewing instructions, searching existing data sources, gathering and maintaining the data needed, and completing and reviewing the collection of information. Send comments regarding this burden estimate or any other aspect of this collection of information, including suggestions for reducing the burden, to Department of Defense, Washington Headquarters Services, Directorate for Information Operations and Reports (0704-0188), 1215 Jefferson Davis Highway, Suite 1204, Arlington, VA 22202-4302. Respondents should be aware that notwithstanding any other provision of law, no person shall be subject to any penalty for failing to comply with a collection of information if it does not display a currently valid OMB control number.

PLEASE DO NOT RETURN YOUR FORM TO THE ABOVE ADDRESS.

1. REPORT DATE (DD-MM-YYYY)		2. REPORT TYPE		3. DATES COVERED (From - To)	
4. TITLE AND SUBTITLE				5a. CONTRACT NUMBER	
				5b. GRANT NUMBER	
				5c. PROGRAM ELEMENT NUMBER	
6. AUTHOR(S)				5d. PROJECT NUMBER	
				5e. TASK NUMBER	
				5f. WORK UNIT NUMBER	
7. PERFORMING ORGANIZATION NAME(S) AND ADDRESS(ES)				8. PERFORMING ORGANIZATION REPORT NUMBER	
9. SPONSORING/MONITORING AGENCY NAME(S) AND ADDRESS(ES)				10. SPONSOR/MONITOR'S ACRONYM(S)	
				11. SPONSOR/MONITOR'S REPORT NUMBER(S)	
12. DISTRIBUTION/AVAILABILITY STATEMENT					
13. SUPPLEMENTARY NOTES					
14. ABSTRACT					
15. SUBJECT TERMS					
16. SECURITY CLASSIFICATION OF:			17. LIMITATION OF ABSTRACT	18. NUMBER OF PAGES	19a. NAME OF RESPONSIBLE PERSON
a. REPORT	b. ABSTRACT	c. THIS PAGE			19b. TELEPHONE NUMBER (Include area code)

PI: Benjamin Vakoc

Title: Characterizing Microvascular Perfusion Kinetics Following Traumatic Brain Injuries

Objective: The goal of this proposal is to characterize the microvascular perfusion kinetics following traumatic brain injury (TBI) using Doppler optical frequency domain imaging. In this proposal, we will develop a windowed model of TBI. Using this model, we will characterize for the first time the critical short (hours) and long (days/weeks) term kinetics of TBI-associated vascular disruption.

Approach: We utilized the following approach to study the microvascular kinetics following TBI.

Optical Frequency Domain Imaging. We have developed an instrument in our lab for assessing the wide-field vascular network in small animal models with high temporal resolution. Additionally, this approach is able to image microvasculature in the wounded brain where the disrupted blood brain barrier prevents fluorescence angiography.

Cranial Window Model of Traumatic Brain Injury. Prior window models of TBI use impact to a metal plate placed on the exposed brain to initiate the TBI. After several days, this plate is replaced with a glass window for imaging. We propose to use the same window for injury initiation and imaging.

Accomplishments: In previous support, we have demonstrated the OFDI can image the TBI site and map vascular morphology longitudinally as the wound expands and heals.

In this work, we have developed a windowed model for traumatic brain injury in mice. After a craniotomy, a polycarbonate impact resistant window is glued permanently to the skull. Impact is provided through a ball-driven piston with an impact force controlled by drop-height. Impact force was measured using piezo-elements to confirm repeatability and scalability of the impact force. The model is most appropriate to mild to moderate TBI.

We observed significant variability in the native vascularization occurring from within the model, and associate this with the quality of the surgical procedure. In cranial windows performed by experienced surgeons, very minimal neovascularization occurs as a result of the surgery. Thus to be able to perform the imaging study, we have hired an animal surgeon with extensive experience to run this program. This staff member will start in the summer, and will lead the imaging effort.

Significance: By understanding the timecourse of vascular disruptions induced by TBI, we can better and more rationally design vascular-targeted interventions. Furthermore, by elucidating the timecourse of microvascular disruption and comparing this with that known in related pathologies such as stroke, common and unique mechanisms driving vascular changes can be identified, which again will guide development of treatment strategies.

Publications/Abstracts:

Mohan N, Vakoc BJ, Principal-component-analysis-based estimation of blood flow velocities using optical coherence tomography intensity signals. Optics Letters 2011;36:2068-70

Patents:

no patents or IP was generated from this proposal.

Principal Investigator: Mei X. Wu, MD, PhD

Project Title: Live Imaging of Perivascular Accumulation of Inflammatory Cells in Injured Brain

Objective: The goal of this proposal is to track cellular responses to traumatic brain injury (TBI) in the brain in a living animal by a novel, in house developed microendoscopy. Our focus was primarily on inflammatory cells that were accumulated in the perivascular space in light of importance of inflammation in both neural recovery and damage.

Approach: Our initial imaging study showed that perivascular accumulation of inflammatory cells occurred only in severely damaged brain. And, only the peri-lesion area could be imaged since the center of the lesion was too much damage to be tracked. Moreover, due to severe brain damage, the mice were not suitable for long-term tracking as they were prone to infection and skin inflammation. In contrast, an increase in the number of pyknotic cells and apoptosis and reduced cell density, in particular, increased activation of microglia, in the cerebral cortex beneath the impact site were apparent hrs after mild TBI (mTBI). The mTBI was induced by closed head injury (CHI) with a weight-drop from 1 cm height onto **non-exposed** mouse skull to protect the mice from skin infection and inflammation. The weight falling height of 2 cm caused mild CHI and 3 cm caused severe CHI. Falling heights of 1 cm merely caused concussion like symptoms at <2 neurological Severity Score (NSS) out of 10. Strikingly, while severe brain damage was associated with a high NSS, the patterns of cellular responses were similar in terms of cell death, cell activation and the degree of pyknotic cells between mTBI and TBI, except for the size of the injured region: the larger the injured region, the higher the NSS would be. We therefore studied cellular responses in the brain subject to mTBI, which would allow us to track cellular responses in a single cell level in a spectrum from brain injury to full recovery.

Accomplishments:

Cell morphology is normalized over time after mTBI: Figure 1 showed that cells became condensed and nuclei were indistinguishable one day after mTBI in the center of the lesion. But on day 28, a significant number of the cells (white arrows) recovered from the injury, as manifested by normal cell morphology similar to those in the controls, concomitant with normalization of neuronal function (NSS<0.5). We are studying whether these injured cells are replaced by normal cells or recover from the injury over time.

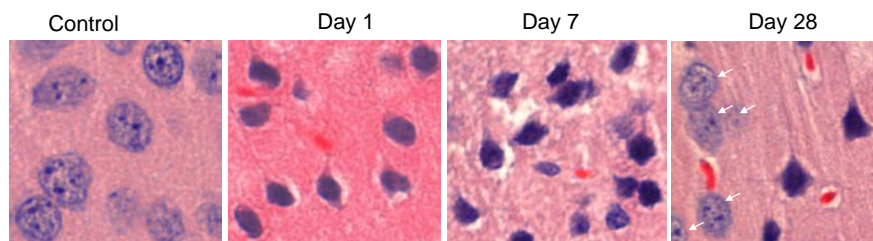
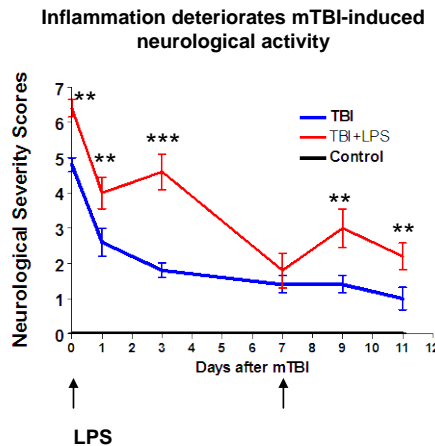


Figure 1. Mouse brain was hit by a pneumatic (cortical) impact device. Histology was examined at indicated days after mTBI.

Inflammation deteriorates neurological function after TBI: Clinical studies have shown that following mTBI, only a small percentage of injured patients (~20%) developed long-term cognitive and emotional difficulties. We hypothesized that other factors like alcohol, inflammation, obesity, high cholesterol may deteriorate neuron damage, causing post-concussion symptoms. We therefore treated mTBI with a high cholesterol diet, LPS to induce

Figure 2. Mouse brain was hit by a pneumatic (cortical) impact device. A low level (100 µg/mouse) of lipopolysaccharide (LPS) was i.p. injected at the same day or 7 days after TBI. Note: an increase in NSS was seen after each LPS injection. **, ***, $p < 0.01$ or 0.001 , respectively; $n = 6$.



inflammatory or induced mTBI in mice with a high level of oxygen reactive species (ROS). We found that both inflammation and a high level of ROS worsened the NSS (figure 2 and data not shown). At the cellular level, the

recovery of cell morphology was delayed accordingly (data not shown)

Microglia activation: During the imaging study, we observed a wide spreading cell morphological alteration, in particular, microglial activation in the lesion and peri-lesion cortex in mice after mild TBI or TBI. Under intravital two-photon confocal scanning microscopy, we observed morphological change of microglia cells from resting ramified form to active “amoeboid” form as early as 6 hr after mTBI. The level of activation correlated with NSS. As shown in figure 3A, under a physiological condition, microglia cells were closely associated with the basal lamina blood vessels. These perivascular microglia cells crowded and moved along on the blood vessel. They were large and extended their dendrite consistently and actively. However, upon mTBI, these microglia cells fell off the blood vessel, fully activated as “bushy”, “rods” or small ameobid shape (Figure 3B). A few of these microglia cells died but most of them moved toward the injure neurons. Significant microglial activation is also a hallmark of TBI in humans and can be detected in patients up to 17 years after TBI (3),

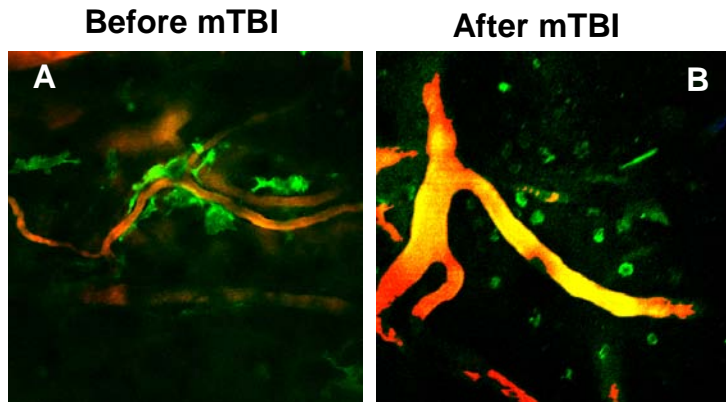


Figure 3. Microglia activation in injured brain (B) as compared to control (A). Mouse brains were hit by a pneumatic (cortical) impact device and imaged by intravital two-photon confocal scanning microscopy via a polished and thinned skull. The mice transgenic expressing MHC-II infused to green fluorescent protein (GFP) were used in the study, which labeled mainly microglia cells in the brain: Green, MHCII+microglia cells; and red, blood vessel stained with dextran red.

stressing a relevance of our observation and an importance of controlling microglial activation at a right time.

Significance: In brief, our study showed significant alteration in cell morphology and behavior in mTBI mice even though the mice were normal in neuronal function, which may serve a better surrogate marker for evaluating the effect of various pharmacological drugs on treatment of this disorder. Further study will be focused on how the injured cells recover and how to speed up the recovery process.

Principle Investigator: Michael R. Hamblin Ph.D.

Co-Investigators: Weijun Xuan, MD, PhD, Quihe Wu, MD, PhD.; Tianhong Dai, Ph.D.; Ph.D.; Ying-Ying Huang M.D.

Project title: Low-level light therapy for traumatic brain injury (TBI)

Objective: Despite many experimental studies and clinical trials, therapies for acute and/or chronic TBI remain elusive. Low-level laser (or light) therapy (LLLT) applied transcranially (from outside the skull) has been used successfully in animal models of stroke and in two human phase 3 trials for stroke. This innovative proposal is designed to test the hypothesis that noninvasive near-infrared transcranial LLLT can be used to treat TBI in the acute and/or chronic settings. Mechanistic studies will be performed using cultured cortical neurons, and LLLT will be tested in acute and chronic mouse models of TBI.

Approach: Embryonic mice were sacrificed to allow primary cortical neurons to be isolated from their brains. These cells can be treated with 810-nm laser and various biochemical and metabolic parameters of cell biology studied. Two different models of TBI in mice were utilized. The first is based on the closed head weight drop protocol of Marmarou et al. It produces a diffuse axonal injury type of TBI with no focal lesion visible on histology. Instead the grey matter tends to be sheared off from the white matter and the tracts of the cortical neurons are deformed. The second was a controlled cortical impact model using a hydraulically driven piston operating through a craniotomy opening to directly impact the cortical surface. This produces a defined lesion in the cortex, which grows in size steadily for 28 days following the injury. Interestingly although the lesion size is increasing over 4 weeks, the neurological performance is steadily improving from a low point immediately after the TBI. This is an example of neuroplasticity by which existing brain cells and circuits can take over the function of damaged parts of the brain.

The basic approach is to shine NIR laser-light (810-nm) on the closed head of the mouse commencing at different times post-TBI, using different power densities, total fluences, pulse structures and most importantly treatment repetition regimens. Various tests for neurological performance, psychological state, and memory and learning are administered to the mice. Mice are sacrificed at different times after LLLT and immunofluorescence studies are conducted for tissue markers of neuroscientific importance in different parts of the mouse brain.

Accomplishments: **Effect of LLLT on oxidative stress in primary cortical neurons.**

Primary cortical neurons were isolated from day 15-16 mouse embryos. Primary mouse neuronal cultures were subjected to three different kinds of oxidative stress. Hydrogen peroxide treatment actually causes oxidative stress by damaging mitochondrial membranes and these remain even after H₂O₂ is removed from the medium. Rotenone inhibits complex I (NADH dehydrogenase) and causes oxidative stress due to interference with electron transport in mitochondria. Cobalt chloride produces a non-mitochondrial type of oxidative stress. In addition to cellular viability, we measured mitochondrial membrane potential as a marker for mitochondrial function, and intracellular ROS by Cell Rox Far Red fluorescent probe. 810-nm

laser was delivered either at 0.3 or 3 J/cm². In all 3 oxidative stresses there was a light dose dependent increase in cell viability showing that NIR light can prevent cell death in cortical neurons. There was a light dose dependent increase in MMP for the CoCl₂ and H₂O₂ but not really for rotenone. Perhaps this was because the MMP was reduced by 80-90% after rotenone treatment and it could not be recovered from this low level by light. The intracellular reactive oxygen species were significantly reduced in the case of CoCl₂ and rotenone and to a lesser extent in the case of H₂O₂, but in this case the rise due to H₂O₂ was not so big. Note that control cells (without oxidative stress) showed a slight but significant increase in ROS upon light delivery in agreement with results we have published previously.

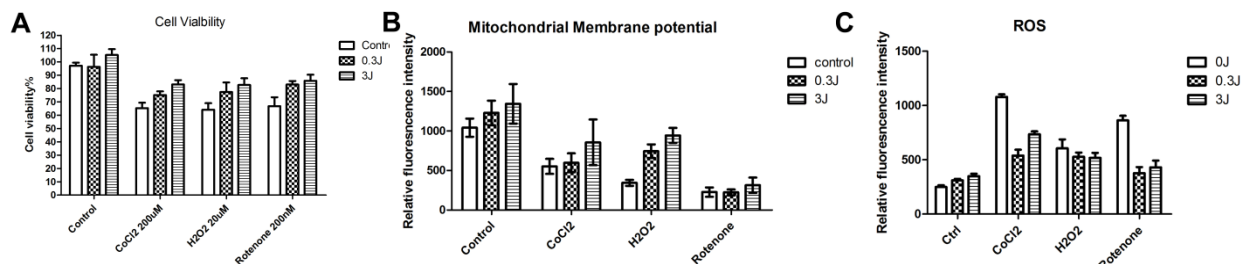


Figure 1. Effect of 810-nm laser on primary cortical neurons subjected to three different kinds of oxidative stress. (A) Viability; (B) mitochondrial membrane potential; (C) Intracellular reactive oxygen species.

The data show that NIR laser therapy can reduce reactive oxygen species in cultured cortical neurons and since ROS are heavily implicated in the pathogenesis of brain damage after TBI, these data suggest a possible explanation of the in vivo findings.

Test the hypothesis that administration of LLLT in the acute period will improve cognitive function and reduce neuropsychiatric sequelae of traumatic brain injury in mice.

We tested LLLT in a mouse model of TBI produced by a controlled cortical impact model that involves making a small craniotomy in the mouse skull and using a pneumatically controlled piston to impact the exposed cortical surface to produce a more localized injury. A single transcranial 810-nm laser treatment (11.7 minutes of 50 mW/cm² delivering 35 J/cm² to the top of the closed mouse head) given 4-hour post-TBI. The principal variable tested in this study was the pulse structure of the 810-nm laser. Different laser pulse parameters were used (CW, 10 Hz with 50% duty cycle and 50 msec pulse duration, or 100 Hz with 50% duty cycle and 5 msec pulse duration). The neurological severity score (NSS) was measured every few days for 4 weeks. NSS is a combined measure of motion, muscle control, alertness and balance. The data are shown in Fig 2A. All three groups of laser parameters had a significantly beneficial effect on NSS over 4 weeks. However while the improvement seen in the CW group and in the 100 Hz groups were roughly comparable, the improvement seen in the 10 Hz group was significantly better than both of them. We also carried out the tail suspension test on the four groups of mice at 1 day and 28 days post TBI. This test measures depression and anxiety-like behavior. As can be seen (Fig 2B) at 1 days post TBI only the optimum 10 Hz laser regimen gave a positive benefit (reduction in immobility time). However at 28 days (Fig 2C) all three laser regimens gave positive benefits with the 10 KHz pulsed laser being the biggest improvement in

psychological state. The explanation for the superiority of 10 Hz pulsing is not immediately apparent, but may be connected to natural rhythms in the brain such as the theta rhythm (10 Hz) in the hippocampus.

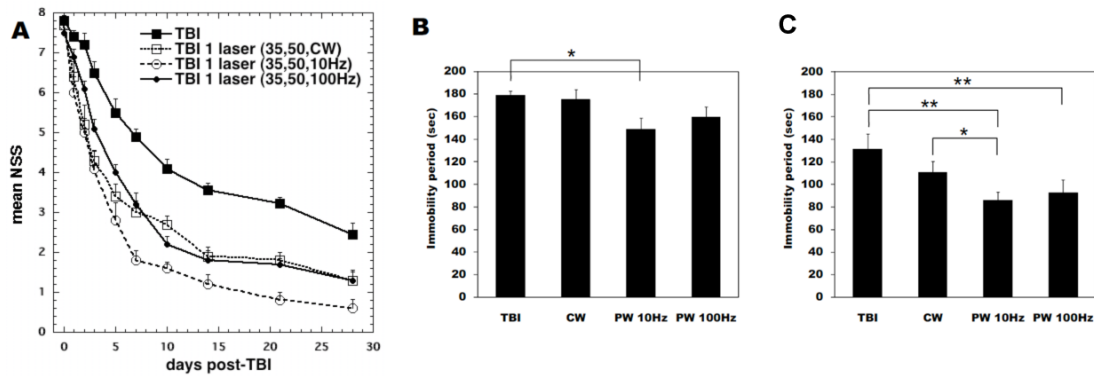


Figure 2. Transcranial 810-nm laser on CCI TBI in mice: effect of laser pulse parameters. A) NSS time course over 4 weeks. (B) Tail suspension test at 1 days and (C) at 28 days.

Mechanisms of action of transcranial LLLT in mouse TBI.

In order to investigate the mechanisms of action of LLLT in TBI we sacrificed mice from the efficacious laser regimen and the sham TBI control at various times after TBI. We also injected BrdU into the mice for 7 days before sacrifice; this compound is incorporated into DNA of proliferating cells and can be readily detected by an antibody. A sample of the data is shown in Figure 3 where sections of the brains removed from TBI mice have been stained with fluorescent antibodies for various markers. are on top row and the corresponding TBI LLLT mice on bottom row. Fig 3A & G show that newly formed BrdU+ve cells (neuroprogenitor cells) which are neuronal in type (Fig 3B&H). Fig 3C&I shows that these BrdU neuroprogenitor cells may be also found in the lesion area. Fig 3D&J shows that caspase 3 expression (an enzyme responsible for apoptosis and cell death of neurons) is reduced in the lesion area and that this might explain the lower size of the brain lesion in mice treated with LLLT. Fig 3E&K show that brain derived neurotrophic factor (BDNF) is upregulated following LLLT to mice with TBI. This may explain much of the beneficial findings. Fig 3F&L show that a marker for synaptogenesis (synapsin-1) is also upregulated after LLLT in TBI. This may explain the increase in neurological functioning after LLLT, even at the same time as the size of the brain lesion is increasing.

Dentate gyrus
of hippocampus

Lesion

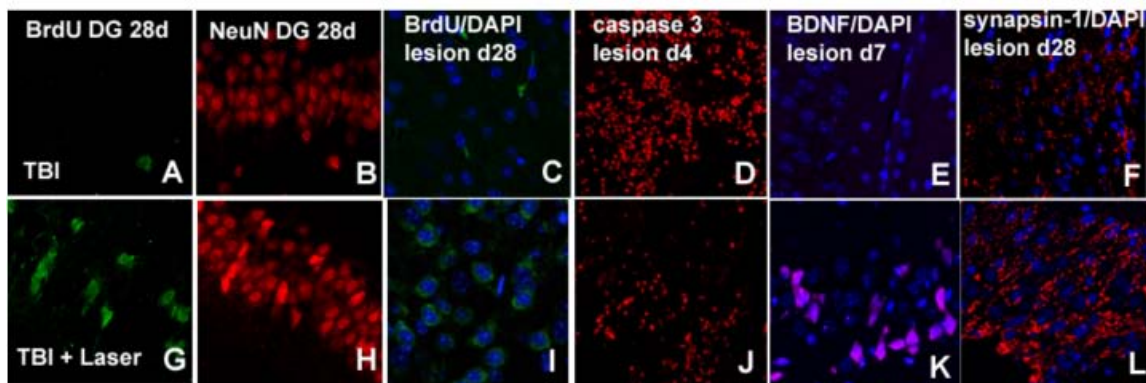


Figure 3. Immunofluorescence of brain sections removed from mice sacrificed at different times after TBI or TBI-LLLT.

Significance: TBI appears to account for a larger proportion of casualties among surviving soldiers wounded in combat in Iraq and Afghanistan, than it has in other recent U.S. wars. As insurgents continue to attack U.S. troops in Iraq, most brain injuries are being caused by improvised explosive devices (IED), and closed brain injuries outnumber penetrating ones among patients seen at Walter Reed, where more than 450 patients with TBI were treated between January 2003 and February 2005. A treatment that is non-invasive, without side-

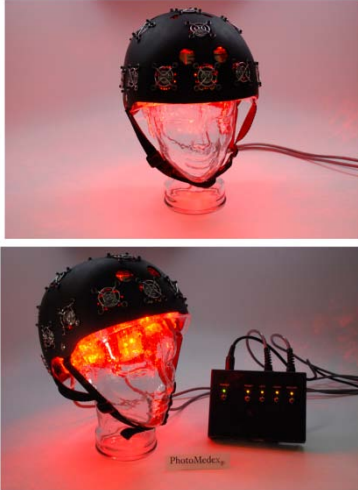


Figure 4. Prototype cap or helmet device with 810-nm LEDs and some 660-nm LEDs capable of delivering 12W total optical power or 40 mW/cm² over the surface of the human head. This would allow a therapeutic dose to be delivered in about 10 minutes.

effects, portable, easily applied by untrained personnel would be of high effectiveness. The “brain cap” shown in Figure 4 could be easily deployed to military hospitals and even combat units.

Publications and Abstracts:

1. Sharma SK, Kharkwal GB, Sajo M, Huang YY, De Taboada L, McCarthy T, Hamblin MR. Dose response effects of 810-nm laser-light on mouse primary cortical neurons *Lasers Surg Med*, 2011, 43(8):851-9. [iereing](#)
2. Naeser MA, Hamblin MR. Potential for Transcranial Laser or LED Therapy to Treat Stroke, Traumatic Brain Injury, and Neurodegenerative Disease. *Photomed Laser Surg*. 2011, 29(7); 443-446.
3. Huang YY, Sharma SK, Carroll JD, Hamblin MR. Biphasic dose response in low-level light therapy – An update. *Dose Response Journal*, 2011, 9(4): 602-618.
4. Ando T, Xuan W, Xu T, Dai T, Sharma SK, Kharkwal GB, Huang YY, Wu Q., Whalen MJ, Sato S, Obara M, Hamblin MR, Comparison of therapeutic effects between pulsed and continuous wave 810-nm wavelength laser irradiation for traumatic brain injury in mice. *PLoS ONE* 6 (2011) e26212-26220.

5. Chung H, Dai T, Sharma SK, Huang YY, Carroll JD, Hamblin MR. The nuts and bolts of low-level laser (light) therapy, *Ann Biomed Eng*, 2011, DOI: 10.1007/s10439-011-0454-7.
6. Kharkwal GB, Sharma SK, Huang YY, De Taboada L, McCarthy T, Hamblin MR. Effects of 810 nm laser on mouse primary cortical neurons. In: Hamblin MR, Anders JJ, Waynant RW, Editors. *Mechanisms for Low-Light Therapy VI*, Bellingham, WA, The International Society for Optical Engineering, Proc SPIE 2011. Vol 7887, 788702
7. Xuan W, Wu Q, Huang YY, Ando T, Huang L, Hamblin MR. In vivo studies of low level laser (light) therapy for traumatic brain injury. In: Hamblin MR, Anders JJ, Waynant RW, Editors. *Mechanisms for Low-Light Therapy VII*, Bellingham, WA, The International Society for Optical Engineering, Proc SPIE 2012
8. Huang YY, Tedford CE, McCarthy T, Hamblin MR. Low level laser therapy reduces oxidative stress in cortical neurons in vitro. In: Hamblin MR, Anders JJ, Waynant RW, Editors. *Mechanisms for Low-Light Therapy VII*, Bellingham, WA, The International Society for Optical Engineering, Proc SPIE 2012

Patents filed for inventions funded, in whole or part, by this award

None

Principal Investigators: Guillermo J. Tearney, MD/PhD, George Velmahos, MD/PhD, Brett E. Bouma, PhD

Project Title: Sensor to identify intra-abdominal bleeding in the field

Objective: Internal bleeding is a major cause of mortality following trauma in both the military and civilian environments. The majority of trauma deaths from bleeding occur in the prehospital or early in-hospital phase, before surgical bleeding control can take place. For this reason, techniques are being developed to allow early post-traumatic bleeding control in the field by paramedics or even untrained personnel. These interventional methods are portable, simple, and safe. However, methods to directly diagnose internal bleeding in the field do not exist. The primary goal of this project is to explore the feasibility of a novel easy-to-use sensor to noninvasively identify intra-abdominal hemorrhage in the field.

Approach: Our method is based on the photoacoustic effect. The patient is irradiated with a short pulse of light. The optical wavelength and pulse duration are selected to selectively excite blood. Upon excitation, the blood-containing region warms up by a few millidegrees, and emits an acoustic wave through the thermoelastic coupling. The resultant photoacoustic wave then propagates back to the tissue surface, and is detected there by a sensitive ultrasonic transducer. Using signal processing techniques, information about the location and dimension of the blood pool are recovered from the temporal profile of the recorded acoustic signal. Photoacoustic excitation is much more sensitive to blood than ultrasound as the generation of the acoustic waves is solely dependent on the optical absorption of blood. Our technique can potentially be performed with portable instrumentation, making it suitable for use by first responders. It furthermore can be rapidly positioned to probe areas more likely to harbor pooled blood.

Accomplishments (9/10-3/12): During this grant period, we developed a bench-top photoacoustic imaging system, proved that it was capable of detecting blood pools in deep tissue and demonstrated its advantage over ultrasonography.

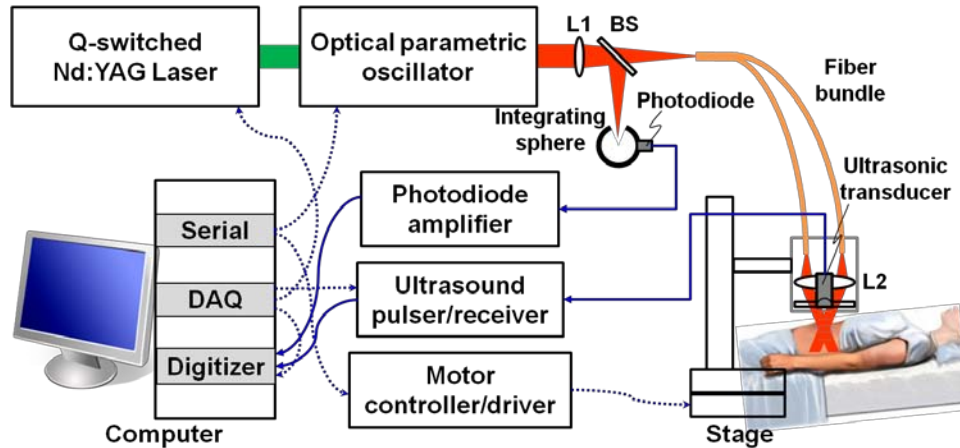


Figure 1: Schematic of the bench-top photoacoustic sensor for intra-abdominal bleeding.

Our bench-top prototype (illustrated in Figure 1) is capable of performing both photoacoustic and ultrasonic imaging of tissue simultaneously. For photoacoustic excitation, a frequency-doubled Nd:YAG laser pumps an optical parametric oscillator (OPO), and generates 5-ns laser pulses at a repetition rate of 10 Hz. The wavelength of the optical excitation can be tuned between 680 and 1000 nm by slightly tilting the BBO crystal in OPO. The light is weakly focused by a lens (L1) and coupled into the proximal port of a high-power silica fiber bundle. In a handheld probe, the light comes out from the eight distal ends of the fiber bundle, which are arranged in a circular pattern. The light is transformed into a Bessel beam by a second lens (L2) to illuminate the tissue. We closely control optical radiation at a safe level in all experiments. For instance, currently at 800 nm, the optical fluence at the tissue surface is estimated to be ~ 7 mJ/cm², which is 5 times lower than the maximum permissible exposure set by the ANSI standard. The generated photoacoustic wave is recorded by a 2.25-MHz piezoceramic transducer, which is placed at the center of the probe. The signal is amplified by a programmable ultrasonic pulser/receiver, and acquired to a computer by a high-speed digitizer at a sampling rate of 50 MHz. In the ultrasonography mode, the same pulser/receiver energizes the ultrasonic transducer to emit short acoustic pulses. The ultrasonic wave backscattered from the tissue is recorded in the same way as the photoacoustic signal. The probe can further be loaded on motorized stages and scanned across the horizontal plane, if cross-sectional and volumetric images of tissue are desirable. A multifunction DAQ card is used to generate multiple triggering signals to synchronize the firing of laser and ultrasonic transducer, the data acquisition and the scanning. A graphic user interface has been written in Labview to enable automatic control of data acquisition and real-time visualization of images.

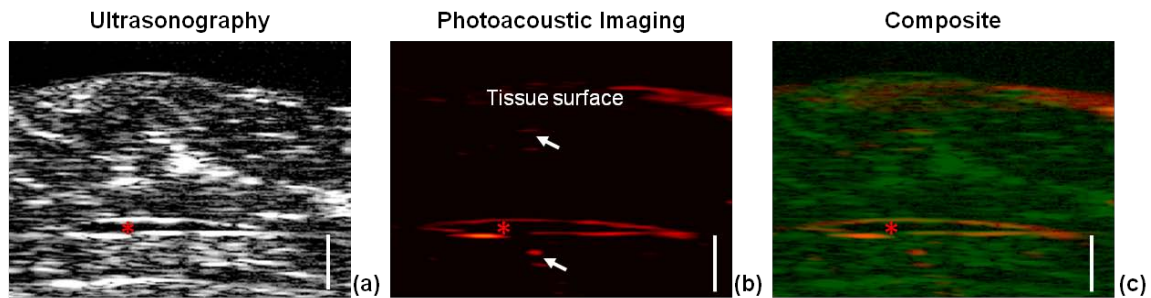


Figure 2: Locating a blood pool embedded in chicken breast tissue. (a) Ultrasonic image. (b) Photoacoustic image using excitation at 800 nm. (c) Composite visualization (photoacoustic image colored in red and ultrasonic image in green). Red asterisk: the blood pool. Arrows: unwanted scattered photoacoustic wave. Scale bars: 1 cm.

A small plastic bag filled with bovine blood was embedded between layers of chicken breast tissue at a depth of ~ 3 cm. We obtained both ultrasonic and photoacoustic images of this phantom in 20 s without any data averaging. The blood pool could be identified as a focal anechoic region on top of a noisy background using ultrasonography (Figure 2a). However, the diagnostic accuracy relies heavily on the selection of system parameters (e.g. gain and dynamic range), and operators' knowledge on normal sonographic appearance of different tissue. Thus, it is difficult to deploy ultrasonography-based internal bleeding detector in the field, where the first responders are mostly inexperienced paramedics and fellow soldiers. By contrast, in photoacoustic image (Figure 2b), the boundary of the blood pool and the tissue surface were clearly delineated over a minimized background. The pseudocolored composite image in Figure 2c further verified that photoacoustic imaging accurately identified the location and size of the blood pool.

Conventional ultrasound imaging cannot differentiate blood from other abdominal fluid, such as serous effusions, leading to a high false positive rate for the diagnosis of intra-abdominal hemorrhage. We anticipated that photoacoustic imaging would be capable of detecting bleeding with much higher specificity, because optical absorption of blood is beyond one order of magnitude higher than water at the selected wavelength (800 nm). We embedded a plastic tube, which is transparent to both ultrasound and light, at a depth of 2.8 cm inside a tissue-mimicking phantom. The tube was

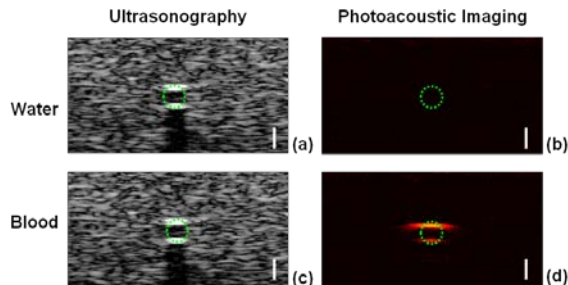


Figure 3: Specificity of bleeding detection. A transparent tube was embedded inside a tissue-mimicking phantom. (b) Ultrasonic and (c) photoacoustic images of tube filled with water. (d) Ultrasonic and (e) photoacoustic images of the tube filled with blood. Scale bars: 1 cm.

sequentially perfused with water and bovine blood. Ultrasonic images (Figures 3a&c), revealed the presence of a tube according to the differential acoustic impedance delineated the tube as a hypoechoic region, but failed to differentiate blood from water. In comparison, photoacoustic images (Figures 3b&d), which map the optical absorption of tissue, enabled the discrimination of blood with a 15-dB higher signal than water.

In summary, we have demonstrated that photoacoustic imaging detects blood pool with a high degree of sensitivity and specificity. This capability could enable diagnosis of internal hemorrhage by first responder in the field. We are now working to further improve the system performance in terms of speed and penetration. The current system is equipped with a single-element ultrasonic detector, thus we have to fire hundreds of laser pulses to obtain a cross-sectional image. Next, we will incorporate a phased array ultrasonic probe, which has 256 parallel detection channels, into the current set-up, and achieve real-time imaging. This modification will also improve the imaging depth by increasing receiving aperture (60 mm vs 6 mm), and implementing synthetic beamforming to numerically focus on every pixel. Also, the photoacoustic wave can be generated from the detector, and reflected by the tissue. This unwanted signal makes it difficult to visualize deep targets (as pointed by arrowheads in Figure 2b). We plan to reduce this source of noise by developing customized probes that reject this reflected light. Lastly, will increase the excitation energy (by 5 times) and perform averaging. After these improvements, we will commence experiments in swine models of internal hemorrhage.

Significance: A portable noninvasive photoacoustic abdominal imaging device will address the unmet challenge of diagnosing internal bleeding in the field by paramedics or even untrained personnel. Combined with early post-traumatic bleeding control methods, our technique can significantly reduce the casualties caused by trauma.

Publications and Abstracts: N/A

Patents filed for inventions funded, in whole or part, by Military Medicine award:

N/A

Principle Investigators: Guillermo J. Tearney, M.D. Ph.D., Brett E. Bouma, Ph.D.

Title: Safe and Cost-Effective Insertion of Percutaneous Tracheostomy in Critically Ill Patients

Objective: Establishment of a definitive airway following respiratory failure is of paramount importance in critically ill patients that often require immediate medical attention for additional ailments. Incorrect intubation can result in significant complications including hypoxemia, regurgitation, aspiration, cardiac dysrhythmia, brain damage, and even death^{1,2}. For these reasons, the standard of care for tracheostomies and endotracheal tube (ETT) intubation in the civilian setting requires a confirmation procedure to prevent inadequate ventilation³. However, the generally accepted tools for confirming proper ETT placement, including direct laryngoscopy and carbon dioxide detectors, are often difficult to implement upon the battlefield, especially for an apneic patient with severe head and neck injuries, thereby making airway compromise the third leading cause of potentially preventable death on the battlefield⁴.

Approach: The development of a miniature, battery-powered sensor within the tracheostomy needle or ETT that could provide red/green/IR light confirmation when a definitive airway had been achieved would be a major step forward in terms of safety and treatment of not only military personnel but the critical-care community at large.

Accomplishments: During the previously funded project, Safe and Cost-Effective Insertion of Percutaneous Tracheostomy in Critically Ill Patients, we investigated the tissues surrounding and within the trachea to identify unique signatures for identifying needle placement during insertion through the neck. However, after discussions with medics and other military personnel, we discovered that cricothyrotomy (CRIC) was an adequate option when ETT intubation could not be achieved. The real needs they described were for intubation guidance to confirm the ETT traversed into the trachea rather than the esophagus, and confirmation the ETT remained engaged to allow the medics to attend to additional critical injuries. We then shifted our focus to discriminating the lumens of the airway and the esophagus in a simple, low-cost device that could integrate within the ETT in Figure 1 such that minimal weight and space would be added to the medic bag.

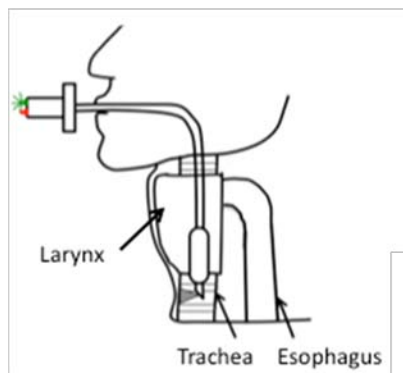


Figure 1: Schematic of guidance device within ETT for intratracheal confirmation.

We discovered during our investigation of optical techniques to identify unique signatures of the trachea and esophagus, that autofluorescence presented the most promise to provide consistent markers within the most compact package. Autofluorescence is the emission of a unique signature of wavelengths dependent on the individual components that makeup the tissue under examination, such as collagen, elastin, and NADH. Figure 2 shows representative fluorescence spectra from the trachea, larynx, and

Figure 2: Fluorescence spectra for trachea, esophagus, and larynx, with 330 nm excitation.

esophagus with 330 nm illumination. From visual inspection of Figure 2 it is apparent that the elastin peak between 400-450 nm and the NADH peak between 450-500 nm is much stronger in the trachea and larynx than the esophagus.

A total of 126 autofluorescence spectra were collected from trachea, epiglottis, larynx, and esophagus excised from 9 swine *en bloc* and separated into airway (epiglottis, larynx, and trachea) and non-airway (esophagus) categories. A principle component analysis was completed on each tissue type and the results were characterized to determine whether the technique could differentiate the location of the sample between the airway and esophagus. Overall the technique presented an 87% accuracy, 97% specificity (95% CI: 84%-100%), and 84% sensitivity (95% CI: 75%-91%) in Table 1. While the overall accuracy and specificity are not yet optimized, incorrectly identifying the airway as the esophagus would instruct the medic to attempt a second intubation or perform a CRIC. The most important parameter is that of the 33 samples acquired from non-airway tissue, only 1 sample was incorrectly identified as the airway.

	Airway	Non-Airway
Fluor+	78	1
Fluor-	15	32

Table 1: Truth table results from 126 autofluorescence spectra acquired from 9 swine samples excised *en bloc* shows 87% accuracy, 97% sensitivity, and 84% specificity.

Significance: A great potential exists for improving the speed and ease of intubation for both the field and civilian critical-care environments with the addition of a miniature autofluorescence device within the ETT. The autofluorescence technique allows for the use of a small, inexpensive light source, such as a light emitting diode (LED), and minimal electronic processing to acquire and process the signals. The miniature form factor could easily fit within current ETTs allowing medics to carry the device without requiring additional space within their bag. If proven successful in a larger follow-up study, such a device would allow an individual medic or untrained officer to follow simple red/green/IR light indicators to guide the ETT down the airway tract without concern for improper ventilation. This device would be an asset for any critical-care scenario to achieve a definitive airway quickly and reliably.

Publications and Abstracts (period 9/10-3/12):

1. Warger WC II, Gardecki JA, Namati E, Suter MJ, Bouma BE, Velmahos GC, Tearney GJ. Needle-probe techniques for trachea identification in tracheostomy procedures. 2011; Photonics West.
2. Warger WC II. Optical techniques for trachea identification. Field Airway Management: Product Line Review 2010.

Patents filed for inventions:

1. Warger WC II, Hancock JL, Gardecki J, Suter M, Velmahos G, Bouma BE, Tearney GJ. Apparatus, systems, methods and computer-accessible medium for identification of trachea.

References:

1. Grmec S. Comparison of three different methods to confirm tracheal tube placement in emergency intubation. Intensive Care Med 2002;28:701-4.

2. Rudraraju P, Eisen LA. Confirmation of endotracheal tube position: a narrative review. *J Intensive Care Med* 2009;24:283-92.
3. Guidelines 2000 for Cardiopulmonary Resuscitation and Emergency Cardiovascular Care: Part 6. Advanced cardiovascular life support: Section 3. Adjuncts for oxygenation, ventilation and airway control. The American Heart Association in collaboration with the International Liaison Committee on Resuscitation. *Circulation* 2000;102:195-104.
4. Mabry RL, Fankfurt A. Advance airway management in combat casualties by medics at the point of injury: a sub-group analysis of the reach study. *J Spec Oper Med* 2011;11:16-9.

Principal Investigator: Charles P. Lin

Project Title: Radiation damage to the eye: cellular response and potential treatment

Objective: Our long-term goal is to understand cellular responses to ionizing radiation in the retina, and to develop appropriate protective or therapeutic measures to mitigate radiation damage. Radiation injury is a potential threat to both military and civilian populations in the event of a nuclear attack. Ionizing radiation is also used medically for tumor treatment and for myeloablation prior to bone marrow transplantation. While radiation is known to affect primarily hematopoietic tissue in the bone marrow, other tissues such as the central nervous system (CNS) can also be affected. Radiation-induced vascular injury (endothelial activation, up-regulation of ICAM-1 and E/P selection expression) can cause peripheral inflammation and even breakdown of blood-brain barrier (BBB). Retina is an extension of the CNS, and the eye is an immune-privileged tissue, but the effect of ionizing radiation to the integrity of the blood-retina barrier (BRB) has not been investigated in detail. Our aims are 1) to identify vascular adhesion molecules responsible for leukocyte-endothelial interaction in the retina using specific antibodies against E-selectin, P-selectin, and ICAM-1; 2) to determine whether dexamethasone, a clinically-used anti-inflammatory drug to reduce side effects of ionizing radiation, can modulate leukocyte-endothelial interaction in the retina; and 3) to develop methods to visualize cell apoptosis in the mouse retina as an early marker of retinal neurodegeneration.

Approach: We have developed a custom confocal scanning laser ophthalmoscope (SLO) for live imaging of the mouse retina. Briefly, the system uses a polygon-based scanning for fast scanning and has three excitation laser sources (491, 532, and 633 nm) and three detectors (PMTs) for simultaneous acquisition of RGB fluorescence images at video rate. Using the SLO, we visualize circulating leukocytes either by transplanting bone marrow cells expressing the dsRed fluorescent protein, or by intravenous injection of a fluorescent dye, rhodamine 6G, that selectively labeled nucleated cells. Leukocyte-endothelial interactions are assessed by quantifying rolling, adhesion, and trans-endothelial migration events in the retinal vasculature. To visualize cell apoptosis in the retina, we collaborate with Dr. David Piwnicka-Worms at the Washington University in St. Louis, who has developed a near-infrared caspase-sensitive probe (KcapQ) with a Cy5.5 fluorophore-quencher pair that is specifically cleaved by caspases in apoptotic cells, resulting in the activation of the fluorescent probe. For these studies we induce apoptosis in one eye by NMDA injection, followed at 22 hours by intravitreal injection of KcapQ into both eyes. Live imaging was performed 6 hours later using the mouse SLO.

Accomplishments (period 9/10-3/12): We have used the custom SLO to examine the expression of cell adhesion molecules on the retinal vascular endothelium. Fluorescently-conjugated antibodies (Ab) against ICAM-1, E-selectin, P-selectin were infused into the circulation by tail vein injection and imaged at 18-24 hours. To verify that binding is specific, a control IgG conjugated to a different fluorophore was co-infused. Figure 1 (left) show a dual color image of retinal vasculature labeled with anti-ICAM-1 (green), which binds to the vascular endothelium, and isotype control IgG (red), which remains in the circulation. Similar results were obtained with anti-E-selectin and control IgG labeling (not shown). The method can be useful for visualizing the up-regulation of adhesion molecules as a potential marker of inflammation and endothelial activation.

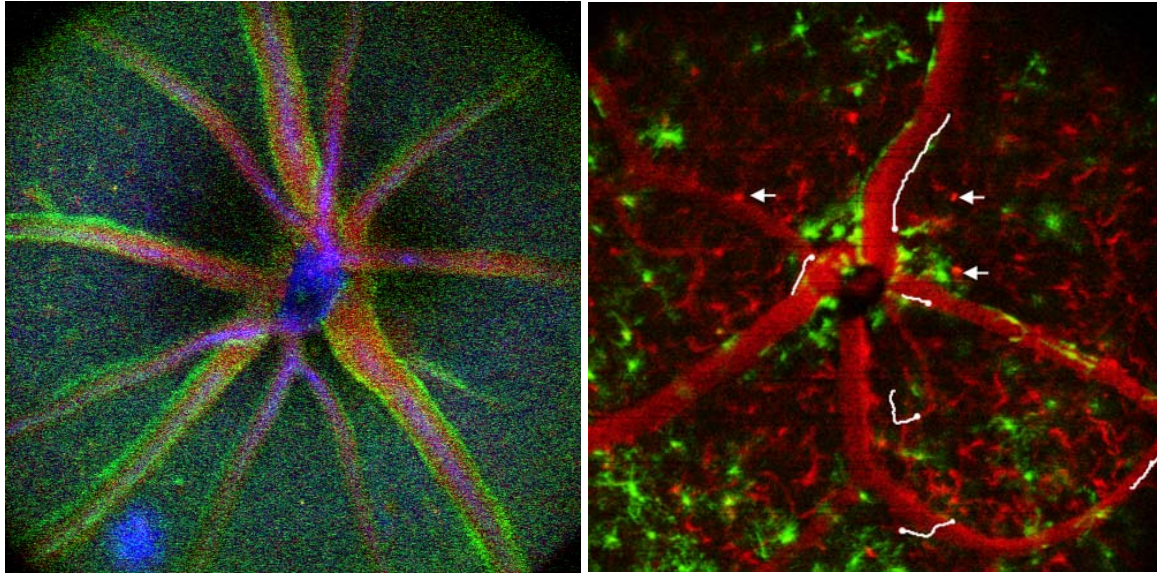


Figure 1. Left – In vivo imaging of ICAM expression on the retinal vascular endothelium (green). The red channel shows the control IgG that is co-infused into the circulation but does not bind to the endothelium. **Right** – Tracks of rolling and transmigrating leukocytes from time-lapse videos.

Tracking leukocyte-endothelial interaction is accomplished by analyzing sequential frames of real-time or time-lapse videos and plotting the position of individual leukocytes as a function of time, as shown in Figure 1 (right, white tracks). We have observed a significant increase in the number of interacting events (at around 10 events per 10-minute time-lapse) in irradiated mice even 15 days post exposure. These interactions are absent in un-irradiated animals.



Figure 2. In vivo imaging of apoptotic cells in the retina, labeled by the caspase sensitive probe KcapQ (Maxwell D et al [Bioconjug Chem.](#) 2009; 20:702-9.)

Figure 2 shows a live image of the mouse retina taken 6 hours after intravitreal injection of the caspase-sensitive probe KcapQ, which should mark the apoptotic cells (green). We are currently optimizing the technique to reduce background fluorescence signal. We will also test a new generation of the caspase sensor (TcapQ) that has been made in Dr. Piwnica-Worms's lab

with significantly better penetration into cells. The specificity of these probes for labeling apoptotic cells need to be validated.

Significance: The live imaging techniques described here will facilitate the development of neuroprotective or therapeutic strategies against retinal/CNS injury by monitoring retinal cell death, inflammation, vascular response in real time. The ability to visualize single cells in the retina of living eyes is also helpful for studying retinal cell biology in situ, thereby improving our understanding of the mechanisms of injury and repair.

Publications and Abstracts (period 9/10-3/12):

1. "In vivo quantification of microglia dynamics with a scanning laser ophthalmoscope in a mouse model of focal laser injury" (SPIE 2012)
2. "In vivo imaging of microglia response to ionizing radiation" (SPIE 2012) - *Received Pascal Rol Award for best ophthalmic technology*

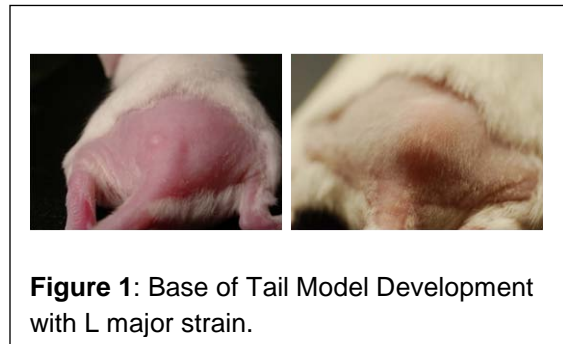
Patents filed for inventions funded, in whole or part, by Military Medicine award (period 9/10-3/12): Lin, Charles P. Retinal Imager for Rapid CNS Inflammation Assessment

Principal Investigator: Tayyaba Hasan, PhD

Project Title: Nanotechnology based topical PDT for cutaneous leishmaniasis

Objective: Photodynamic therapy (PDT) is a therapeutic approach based on the photo-oxidation of biological materials induced by non-toxic chemicals called photosensitizers (PSs). The PS preferentially localizes in certain diseased cells and these cells are destroyed when illuminated by a light of the right wavelength and at a sufficient PS dose. PDT has evolved as a promising therapeutic modality for the treatment of cutaneous leishmaniasis (CL). The first clinical study of PDT for cutaneous parasitic infections showed that PDT promotes relatively faster localized healing of the diseased lesion. The broad objective of present study was to develop a topical PDT regimen using nanotechnology and hydrogels for the management of CL in a base of tail ulcer model. Specifically, the objectives were to design and synthesize formulations and establish treatment efficacy in vivo in a murine base of tail (BT) model of CL.

Approach: Nano formulations of Photosensitizer EtNBS were synthesized, purified, and characterized using dynamic light scattering. Nanoconstructs with an average size of 106 nm (PDI 0.06) were obtained and studied for their photokilling efficacy.



For in vivo BT study, 6-8 weeks old female BALB/C mice were infected with 1×10^6 metacyclic promastigotes of *L. Major (old world)* strain of Leishmania. The infection was allowed to develop for 3-4 weeks (Figure 1).

Accomplishments (period 9/10-3/12): PDT could be a promising therapeutic modality for the treatment of CL. The first clinical study of PDT for cutaneous parasitic infections showed that PDT promotes good localized healing of the diseased lesion although the number of treatments required was high.

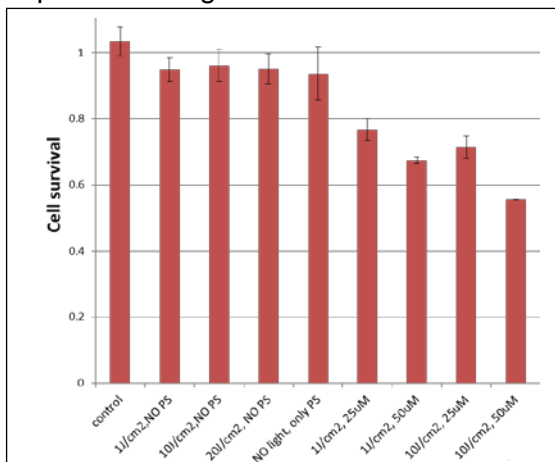


Figure 2: PDT of *L panamensis*.

After a successful scanning of available photoactivatable drugs, we have selected the most potent agent for further evaluation in a nanotechnology based delivery vehicle. We have developed a polymer/liposomal encapsulated photoactive agent with shows improved penetration and treatment efficacy in cell culture experiments.

To investigate the new construct in an appropriate animal model of infection, we have developed a base of tail model which more closely replicates the human form of infection using both Leishmania

major (LM) and Leishmania panamensis (LP). The LP was found to be much more resistant to all treatments (Figure 2).

Significance: If successful we anticipate that this research will culminate in a new paradigm for a convenient and safe treatment of leishmaniasis. PDT is efficient and well-tolerated by the patients. PDT is a desirable parasite killing modality because parasites and microbes resistant to standard treatments are responsive to PDT. While the dynamics of treatment may be somewhat different in humans, we hope that our study with comparison on site of infection and type of formulation will provide a useful starting point for the optimization of topical PDT applications for granulomatous infections.

Publications:

1. Oleg E. Akilov, Ulysses W. Sallum and Tayyaba Hasan. PDT for Cutaneous Leishmaniasis in Photodynamic Inactivation of Microbial Pathogens: Medical and Environmental Applications. Ed: Editor(s): Michael R Hamblin, Giulio Jori. RCS Publishing 2011.
2. Latorre-Esteves E, Akilov OE, Rai P, Beverley SM, Hasan T. Monitoring the efficacy of antimicrobial photodynamic therapy in a murine model of cutaneous leishmaniasis using L. major expressing GFP. J Biophotonics. 2010; 3(5-6):328-35.

Patents filed for inventions funded, in whole or part, by Military Medicine award (period 9/10-3/12): N/A

Investigators: Andy Yun (P.I.), Charles P. Lin, Georges Tocco*, Gilles Benichou*

* Surgery/ Transplantation Unit, Massachusetts General Hospital

Title: In Vivo Study of Viability and Tolerance for Skin Transplantation

Objective: The long-term goal of this project is to develop novel skin transplantation methods to help wounded soldiers. While long-term survival/tolerance of vascularized organ transplants, such as kidney and heart, can be relatively easily achieved, presently there is no suitable treatment that would result in the long-term survival of allogeneic skin grafts.

The first specific aim of this project is to test the feasibility of using frozen skin in allogeneic murine models. The second specific aim of this project is to evaluate the effect and mechanism of APC depletion and antibody treatments for long-term graft survival. The third specific aim of this project is to investigate the role of vascularization in skin transplantation and the possibility of promoting tolerance induction in vascularized allografts.

Approach: We used skin transplantation in mice as a model. We tested two methods to promote prolongation and tolerization of allogeneic skin transplants: (i) use of frozen skin for partial matching; (ii) removal of antigen presenting cells from the donor graft, and (iii) use of skin vascularization at transplantation time combined with tolerization protocols that are known to work in other organ (vascularized) transplants in the same species.

We compared the alloimmunogenicity, susceptibility and cellular trafficking associated with transplantation of fully allogeneic conventional non-primarily vascularized skin grafts and skin allografts vascularized at the time of their placement on mice (vessel anastomoses at time of grafting, see fig. 1).



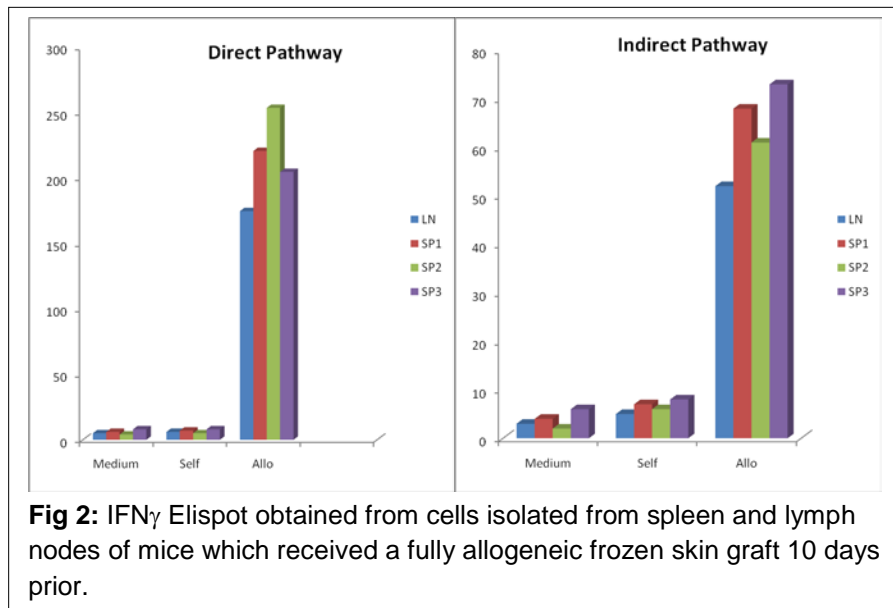
Fig. 1: Vascularized skin flap at the level of the groin area where the donor skin epigastric arteries and veins are anastomosed (end to end for arteries and end to side for veins) to the recipient femoral arteries and veins.

Accomplishments (->9/10):

i) Use of frozen skin for transplantation in allogeneic murine combinations

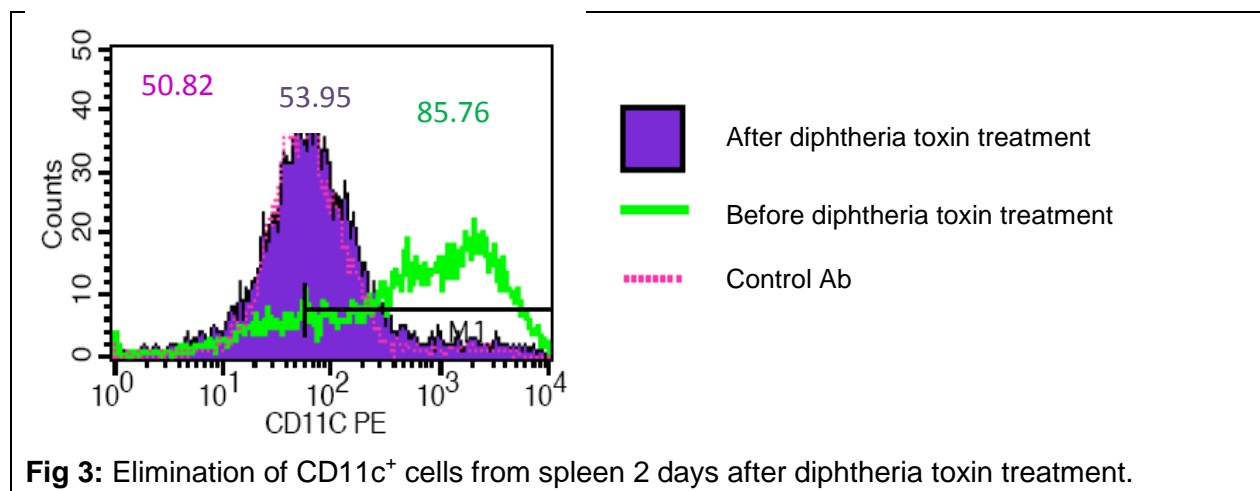
We tested 2 different methods for freezing skin, 15% DMSO and 20% glycerol. In our hands, skin frozen in glycerol as a source of skin transplants generated a rejection time and immune response similar to that observed with freshly prepared skins (measured by Elispot analysis,

see fig 2). Ideally, it would be beneficial to have access to an apparatus that enables a gradual freezing of the skin at a rate of 1°C/min to avoid tissue damage due to crystal formation.



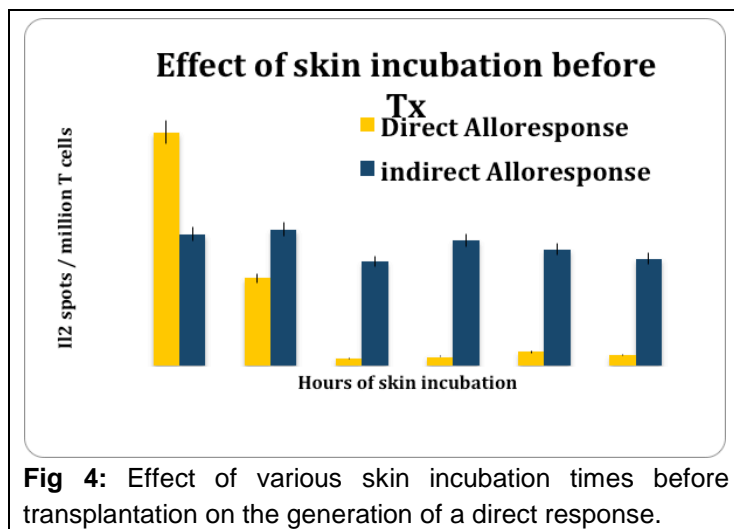
ii) Evaluate the effects and mechanisms of APC depletion for long-term graft survival

The approach used here was to use CD11c-GFP-DTR transgenic mice as skin donors. These mice carry the receptor for diphtheria toxin on the cells that are positive for CD11c (a specific marker for dendritic cells). Mice do not normally express a receptor for diphtheria toxin, so when Diphtheria toxin is administered to these mice, only the CD11c positive cells are transiently eliminated. However the treatment can only be administered 2 times in a row and the DC population eventually comes back. We used this method to eliminate transiently the CD11c positive cells from the transplant with the idea that this treatment would slow down induction of the immune response (through the direct pathway). Fig 3 shows the elimination of CD11c+ cells after treatment of CD11c-GFP-DTR transgenic mice with diphtheria toxin.

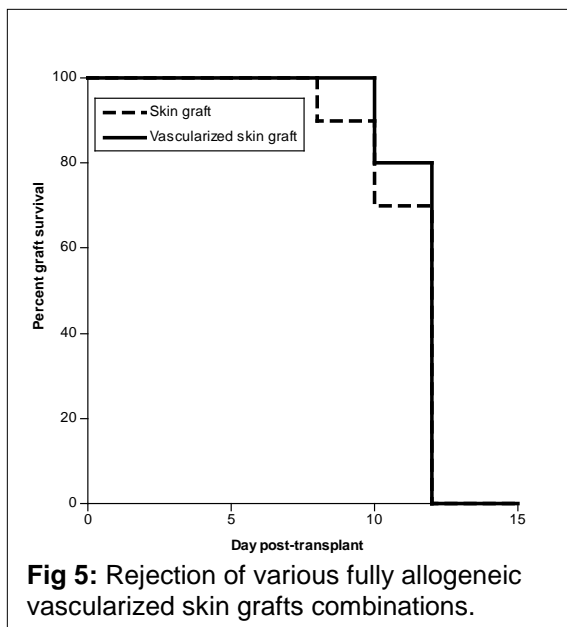


While the treatment was successful in eliminating the dermal DCs from the donor skin (observed through in vivo microscopy), it did not delay the rejection nor did it have an impact on the immune response. One possible explanation for this lack of effect might be the fact that the treatment did not eliminate the Langerhans cells from the donor skin (observed through in vivo microscopy). Langerhans cells represent a dendritic cell population present in the epidermis of the skin. We would therefore need to eliminate these cells through another method to ascertain if elimination of donor APCs might prolong/help tolerize skin grafts.

Pre-incubating the skin graft in culture medium before actual transplantation is effective in depleting the graft from DCs. The APCs during the incubation time do migrate out of the graft in the culture medium. This treatment was then successful in delaying the skin graft rejection and preventing activation of the direct pathway (Fig. 4). We would therefore envisage a situation where prior to freezing, skin graft would be pre-incubated in culture medium for 24-48 hours prior.



iii) Investigate the role of vascularization in skin transplantation and the possibility of promoting tolerance induction in vascularized allografts

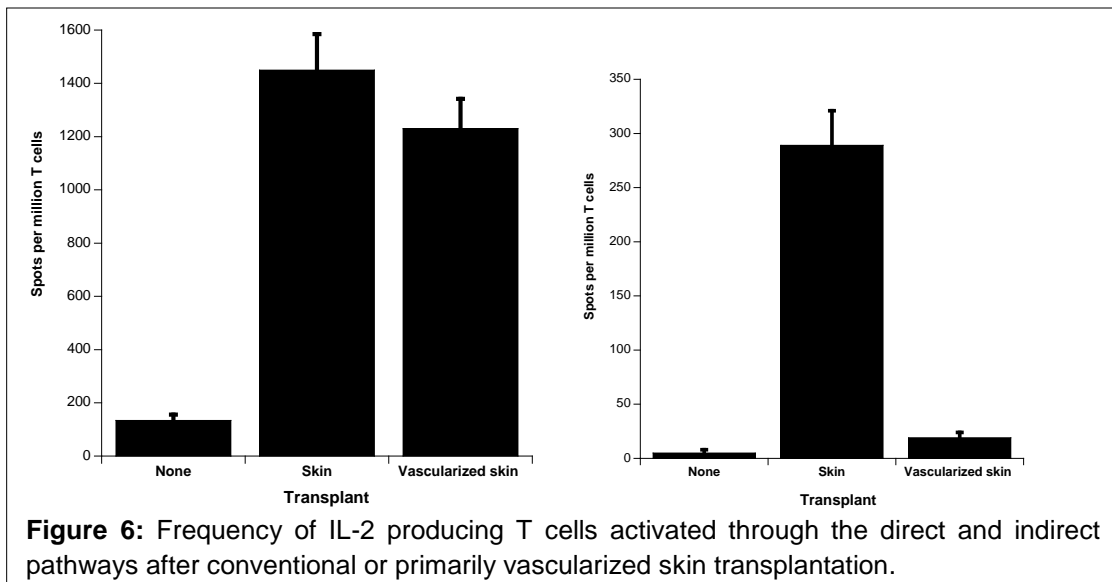


We compared the cell trafficking, T cell allorecognition and susceptibility to tolerogenesis in mice transplanted with a fully allogeneic “classical” skin graft and recipients of a skin allograft vascularized at the time of its placement. First, we evaluated the acute rejection of various skin allografts combinations, vascularized at the time of their placement and conventional, non-primarily vascularized, skin allografts in mice. Vascularized skin grafts were acutely rejected although in a slight but not significantly delayed manner compared to conventional skin grafts (see fig. 5)

We observed that graft vascularization at transplantation time is associated with a totally different pattern and kinetics of passenger leukocyte migration (immune cells from the graft). In table 1 are reported the number of passenger leukocytes from the donor that are retrieved in various tissues of the recipient at various time points after transplantation. We observed that after vascularized skin grafts, as early as 1 day post-transplant, passenger leukocytes from the donor are retrieved in all the secondary lymphoid organs that we observed. Contrary to expectations, after conventional skin transplantation, only few passenger leukocytes are retrieved only in the draining lymph node of the recipient and only after 5 days post-transplant.

Days post Tx	Skin					Vasc Skin	
	1	3	5	7	9	1	3
Spleen	0	0	0	0	0	26	54
Thymus	0	0	0	0		0	0
Lung	0	0	0	0		0	0
Liver	0	0	0	0		0	0
Mes LN	0	0	0	0	0	256	80
Draining Ing LN (ipsi)	0	0	8	4	0	6	4
Paraortic (ipsi)	0	0	0	0	0	0	6
Draining Axill (ipsi)	0	0	6	0	0	42	18
Bracchial (ipsi)	0	0	0	0	0	ND	18
Cervical (ipsi)	0	0	0	0		22	20
Ing LN (contra)	0	0	0	0	0	34	20
Paraortic (contra)	0	0	0	0	0	6	8
Axill (contra)	0	0	0	0	0	94	38
Bracchial (contra)	0	0	0	0	0	28	14
Cervical (contra)	0	0	0	0		22	20

Vascularized skin transplants are also associated with a different alloresponse by T cells, the recipient immune cells in part responsible for the ultimate rejection of the graft. No indirect



response could be measured after vascularized skin transplantation (see fig. 6).

In addition, we found that unlike their non-vascularized counterparts, primarily-vascularized skin allografts become infiltrated very early on by large numbers of regulatory T cells (cells specialized in dampening/eliminating the immune response, data not shown).

Finally, we studied the effect of a tolerization protocol known to be effective with heart transplant. Short-term treatment of recipients with anti-CD40L monoclonal antibodies (MR1) has been shown to prolong the survival of heart but not skin allografts. The effect is known to rely essentially on the inhibition of alloreactive CD4+ T cells. First, we compared the effect of anti-CD40L mAbs (0.5 mg injected I.P. at day 0, 2 and 4) on the rejection of non-vascularized skin allografts, vascularized skin allografts and cardiac allografts in the B6 to C3H combination. As expected, anti-CD40L-treatment had no significant effect on the survival of non-vascularized skin allografts. In contrast, preliminary results show that this treatment can markedly extend the survival of vascularized skin transplants.

Vascularized skin allografts can enjoy long-term survival when combined with a short term treatment with an anti-costimulation blockade antibody.

These results bring new insights into the mechanisms by which vascularization influences the immunogenicity and tolerogenicity of allogeneic skin transplants. They open new hopes for one day being able to achieve long-term survival of allogeneic skin grafts for soldiers.

Significance: The results obtained up to now are encouraging about the potential for vascularized skin in achieving long-term graft survival and tolerization. The exact mechanism of the prolonged survival of vascularized graft is unknown at the moment. If successfully developed, vascularized skin transplantation might prove useful to treat wounded soldiers in the battlefield and during rehabilitation.

Publications and Abstracts (9/10-3/12):

1. Tocco G., Kim P., Kant CD., Lin C., Yun S., Benichou G., "Cellular Migration in Transplantation Studied Using in vivo Microscopy.", *Clin Immunol.* 131: S11-12, 2009.
2. Tocco G., Kim P., Kant CD., Wynn H, Lin C., Yun S., Benichou G., "The ins and outs of Cellular Migration in Transplantation Revisited through *In Vivo* Microscopy." *A. J. Trans.* 9: P476, 2009.
3. Tocco G., Kant CD., Kim P., Connolly SE., Shea S., Lin C., Yun SH., Benichou G., "Skin Graft Rejection: Direct or Semi-Direct Allorecognition?", Annual Scientific Exchange December 3-6, 2009, Orlando, Florida.
4. Tocco G., Kim P., Kant CD., Lin C., Yun SH., Benichou G., "Allorecognition after Skin Transplantation: Potential for Semi-Direct Pathway?" *A. J. Trans.* 10: P94, 2010.

Patents filed for inventions funded, in whole or part, by Military Medicine (AFOSR) (9/10-3/12): None

Principal Investigators: Irene E. Kochevar, Robert W. Redmond, Min Yao

Project Title: Improved method for covering burn injuries with grafts

Objective: Burn injuries are a frequent component of battlefield trauma. All deep partial-thickness and 3rd degree burns require skin grafts. Currently grafts are attached with sutures and staples at the graft edges that further damage the underlying tissue and initiate excessive scarring and do not specifically prevent dehiscence at the center of the graft. The objective of this project was to improve the method for attaching skin grafts and alternative coverings that causes minimal tissue trauma while achieving maximum success rate and producing minimal scarring.

Approach: To avoid or minimize the use of scar-inducing sutures and staples for attaching skin grafts, we used a light-activated technology that bonds tissue surfaces together by forming protein-protein crosslinks to bridge the tissue planes. This method, called Photochemical Tissue Bonding or PTB, uses a safe dye and clinical green laser and had previously been shown to adhere skin grafts to dermis ex vivo¹. Our studies have shown that PTB does not damage tissue and decreases scarring/fibrosis in several animal studies²⁻⁵.

The specific aims were: (1) To determine the light fluences and irradiances that were required for PTB to securely attach split-thickness skin graft (STSG) or/and a composite skin graft in a porcine model for skin burn injury. (2) To determine relative advantages of using PTB versus sutures for STSG or composite skin graft attachment. Outcome measures included procedure time, ease of use, success rate and parameters of healing.

Accomplishments (period 9/10-3/12): Studies to determine the light fluences and irradiances required to attach STSG were carried out using 2 cm x 2 cm full-thickness wounds in swine skin as a model for burn injury. The surface of the wound beds was stained with 0.1% Rose Bengal dye, then the grafts were placed in wound beds and treated with green light (LED or KTP laser). Two irradiances (0.10 and 0.20 W/cm²) were tested at fluencies of 10 and 25 J/cm², and 0.10 W/cm² was used to deliver 50 J/cm². The shortest and longest irradiation times were 50 seconds and 8 minutes 20 seconds. One-way ANOVA showed that there was no significant difference in graft scoring items including color, bonding, dislocation and hematoma amongst all groups on day 3 and 7 ($P>0.05$). The laser and LED increased the temperature similarly, both were not over 40.5 °C and no difference in grafts adherence ($P>0.05$).

Based on these results, a fluence 25 J/cm² delivered at 0.10 W/cm² was selected for bonding studies using larger grafts (4 cm x 5 cm). On day 3, the color and hematoma of grafts in PTB group was significantly better than those in suture groups ($P<0.05$). On day 7, the graft color in PTB-treated sites was still better than that in suture group ($P<0.05$). On days 10 and 14, there was no difference between PTB and suture groups in the scoring of grafts.

The average procedure time for attaching grafts with PTB (4 min, 10 sec) was three-times shorter than attachment with sutures. There was no significant difference between PTB and

suture groups on wound contraction rate ($P>0.05$). Sutures produced greater inflammatory infiltrate on day 7, 10 ($P<0.001$) and day 14 ($P=0.006$) than observed in the PTB groups.

Significance: These results indicate that PTB secures split thickness skin grafts to wound beds with better outcomes than sutured attachment. The shorter time required for attachment translates into shorter overall procedure times. The significantly lower level of inflammation after PTB attachment will result in less scarring at the graft edges. Both of these factors represent improvements over the current methods for skin graft attachment.

Publications and Abstracts (period 9/10-3/12): None

Patents filed for inventions funded, in whole or part, by Military Medicine award (period 9/10-3/12): None

References:

1. Chan BP, Kochevar IE, Redmond RW. Enhancement of porcine skin graft adherence using a light-activated process. *J Surg Res* 2002;108:77-84.
2. Henry FP, Goyal NA, David WS, et al. Improving electrophysiologic and histologic outcomes by photochemically sealing amnion to the peripheral nerve repair site. *Surgery* 2009;145:313-321.
3. Johnson TS, O'Neill AC, Motarjem PM, et al. Photochemical tissue bonding: a promising technique for peripheral nerve repair. *J Surg Res* 2007;143:224-229.
4. O'Neill AC, Randolph MA, Bujold KE, et al. Preparation and integration of human amnion nerve conduits using a light-activated technique. *Plast Reconstr Surg* 2009;124:428-437.
5. Tsao S, Yao M, Tsao H, et al. Light-activated tissue bonding for excisional wound closure: a split-lesion clinical trial. *Br J Dermatol* 2012;166:555-563.

Principal Investigators: Hensin Tsao, M.D., Ph.D. (At MGH), Pablo J Prado, Ph.D. (At One Resonance, LLC)

Project Title: Development of a Portable Hand-held Magnetic Resonance Device for Skin Surface Analysis.

Period: 9/2010 to 3/2012

Objective: *Broad Goal:* The long-term objective of the project is to introduce a portable, combat-friendly hand-held open magnetic resonance (MR) device to improve point-of-care diagnostic capabilities through minimally invasive technologies.

Specific Program Goals: Design, fabricate, and test a single-sided magnet array providing magnetic field distribution suitable for scanning skin tissue up to 3 mm in depth.

Approach: Various configurations may be considered to provide a portable MR instrument for in-situ diagnostics although many previous approaches have been fraught with challenges:

1. Compact MRI machines: they require cryogenic cooling and weigh hundreds of pounds. This approach has been limited to the imaging of arms and legs at dedicated clinics.
2. Portable magnet with selected sensitive volume: requires displacement of probing head. Requires mechanical components that control the positioning of the probe. Calibration, size and complexity are issues for these configurations. This approach has been limited to material analysis in the laboratory
3. Hand-held probe for localized evaluation: Automatically generates a localized depth profile of the tissue using a portable instrument



The hand held configuration is the proposed solution from One Resonance. A compact console has been used for the measurements presented below.

Accomplishments (Period 9/10-3/12): A hand-portable MR probe was developed to perform localized tissue analysis by placing the probe on the region of interest and observing the MR response from skin tissue several millimeters in depth.



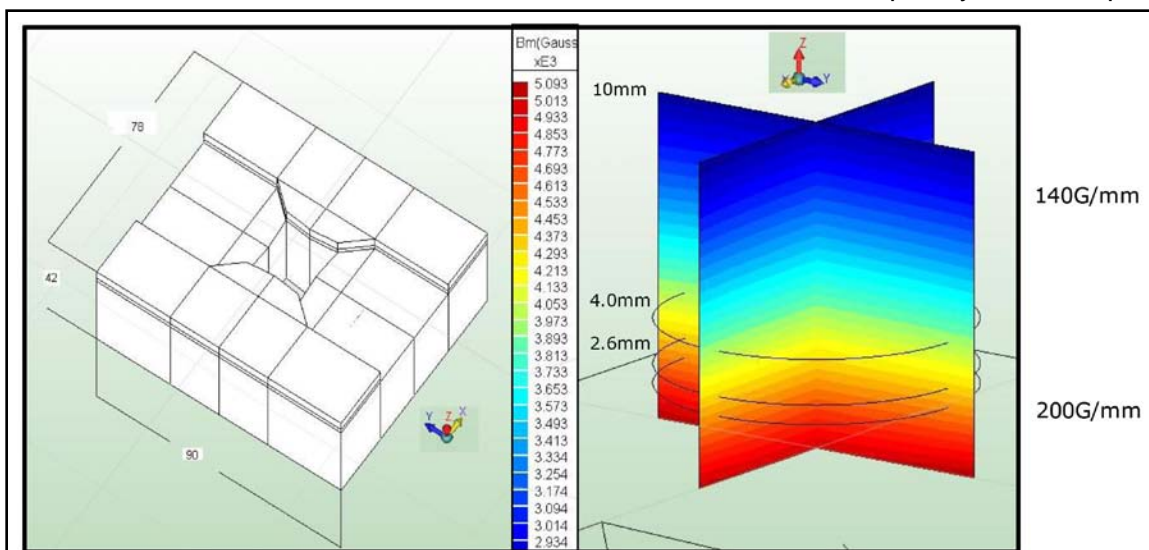
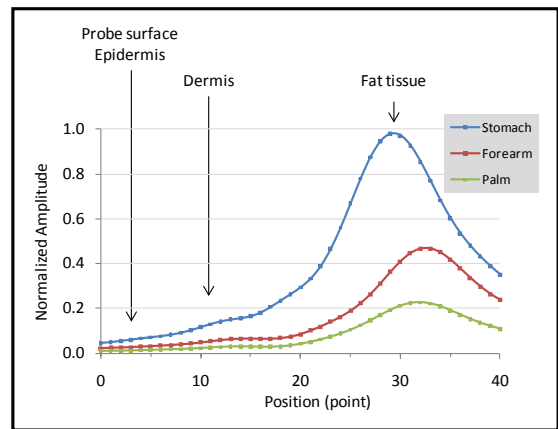
Significant advances were made in the development of a hand-portable MR instrument, towards providing depth discrimination (T_1 and T_2 weighted profiles):

A new single-sided radio-frequency coil was used

in combination with a compact open magnet. The open magnet was constructed prior to the current research phase using pre-shaped blocks of high grade permanent magnets. The magnet array generated effectively flat surfaces of constant magnetic field above the probe. The new flat, double-layer solenoid RF coil was placed on top of the magnet to project fields in the sensitive region, above the probe.

Depth resolution of the skin was achieved in-vivo.

The figure below shows scans over various areas of the PI's body. T_2 and density-weighted depth resolution was achieved using a series of CPMG echoes in the presence of large static field gradients. The time domain data was Fourier transformed to attain frequency-encoded profiles



in a similar manner to conventional MRI. It is noted that widely used interventional clinical MRI units use a similar level of static magnetic field as the open probe.

The open hand-held open MR probe collects signal with a method based on stray field imaging and inside-out MR. Deeper penetration depth may be achieved by switching the excitation

frequency and receiver resonant frequency. [Prado PJ. Single-Sided Imaging Sensor. Magn. Reson. Imaging, 2003, 21, 397-400]

A custom magnet generating flat surfaces of constant magnetic field needs to be fabricated to achieve proper depth resolution. See the proposed model below.

Next Steps

1. Evaluate tissue discarded during surgery: MR contrast
2. Use probe optimized for depth profiling and evaluate depth resolution of the scan. Use a series of phantoms simulating the MR response of skin tissue and pools of blood
3. Propose configuration for diagnosis of superficial and medium depth lesions resulting from combat injury or exposure (e.g. extremity and subdural hematomas, internal hemorrhage, and soft tissue infection)

Significance:

Portable diagnostic devices have become essential components of military and civilian medicine. Within the military context, an open-configured, easily deployable and diagnostically reliable MR device would be an ideal field adjunct in the diagnosis and monitoring of superficial and medium depth lesions resulting from combat injury or exposure (e.g. extremity and subdural hematomas, internal hemorrhage, and soft tissue infection). MR signals may also prove more effective at delineating perfusion or oxygenation status- crucial parameters that could lead to earlier life-saving measures.

Publications and Abstracts (period 9/10-3/12): None

Patents filed for inventions funded, in whole or part, by military medicine award (period 9/10-3/12): None

Principal Investigator: Robert W. Redmond PhD

Project Title: Augmented repair of Achilles tendon rupture with biocompatible nanofiber matrix.

Objective: The purpose of this study was to test the hypothesis that a combination of a new nanofiber biomaterial with a light-activated fixation technique could provide a strong supporting structure at the repair site during early wound healing that would promote organized healing and reduce adhesion formation in a rabbit model of Achilles tendon repair.

Approach: Surgical re-attachment of tendon provides a secure repair and is indicated for patients wishing to return to full physical activity, but complications such as infection, inflammation, adhesions and scarring can frequently result. Suture repair provides sufficient mechanical strength to the tendon during re-attachment and healing to prevent re-rupture but the prolonged period of immobilization that protects the vulnerable tendon from re-rupture during healing is associated with poorer functional outcomes. Earlier mobilization of the joint is now thought to be advantageous in reducing adhesion formation, reducing calf muscle wastage and minimizing deep venous thrombosis and improves functional outcomes. Photochemical tissue bonding (PTB) has been investigated as a new approach for wound closure or tissue repair in several tissues. PTB is a potential alternative to mechanical fixation techniques with advantages including the formation of a strong, water-tight seal, and PTB does not promote the inflammation, foreign body reaction and scarring caused by sutures.

We investigated an augmentation of tendon repair using PTB to bond a strong supporting biocompatible sleeve around the repair site with a possible reduction in suture burden. A stronger and less expensive material that could be mass-manufactured and used as a photochemical graft material could greatly enhance the efficacy and adoption of PTB in orthopedic practice. Thus, we explored an electrospun silk mat (ES) as a new nanofiber biomaterial for PTB. Silk is similar in chemical structure and composition to collagen, and electrospinning silk fibroin is a controlled method for generating fibrous silk with high selectivity of fiber diameter and alignment, pore size and material thickness. We have prepared ES mats using random or aligned fibers that, when bonded over the tendon repair site, could reduce the tensile load across the healing tendon and influence wound healing. ES shows good biocompatibility with limited immunological activity and can act as a scaffold to support cell attachment and proliferation. Thus, silk presents an attractive, inexpensive material for use as a PTB-affixed repair augmentation. Outcomes tested included biomechanical strength of repair, PSOFDI imaging of neo-collagen fibers, extent of adhesions and histological examination of the healed tendon as a function of post-operative time.

Accomplishments: Silk fibroin was extracted from silk cocoons and purified before electrospinning into fibrous mats. SEM images of ES mats showed fiber diameters of 690 ± 260 nm mimicking the architecture of the ECM (50-500 nm) with the benefit that these larger fibers can sustain larger forces. New Zealand white rabbits underwent surgical transection of the Achilles tendon and repair by, (a) SR; standard Kessler suture + epitendinous suture (5-0 vicryl). (b) ES/PTB; a single stay suture and a section of ES mat, stained with 0.1% Rose Bengal (RB), wrapped around the tendon and bonded with 532 nm light ($0.3\text{W}/\text{cm}^2$, $125\text{ J}/\text{cm}^2$).

(c) SR+ES/PTB; a combination of (a) and (b). Gross appearance, extent of adhesion formation and biomechanical properties of the repaired tendon were evaluated at days 7, 14 or 28 post-operatively (n=8).

Ultimate stress (US) and Young's modulus (E) in the SR group were not significantly different from the ES/PTB group at days 7, 14 and 28, post-operatively. Adhesions were considerably greater in the SR group compared to the ES/PTB group at days 7, 14 and 28 ($p < 0.0001$). The combination approach of SR+ES/PTB gave the best outcomes in terms of E at 7 ($p < 0.016$) and 14 days ($p < 0.016$) and reduced adhesions compared to SR at 7 ($p < 0.0001$) and 14 days ($p < 0.0001$), the latter suggesting a barrier function for the photobonded ES wrap.

In subsequent studies the ES mat was prepared with aligned silk fibers (ESA) that were photobonded to the tendon in alignment with the natural tendon fibers. The aligned nanofiber mat possesses greater mechanical strength than the random mat. In a rat model of Achilles tendon transection the photobonded ESA augmentation provided greater mechanical strength to the repair while maintaining the adhesion barrier function seen in the random ES mat. Histology showed lower inflammation in the photobonded mat compared to standard Kessler suture repair. Polarization sensitive, optical frequency domain imaging (PSOFDI) of healing tendons in the proliferative phase of wound healing (14 days post-op) showed new collagen fibers being laid down in an organized structure like native tendon, whereas suture repair leads to random collagen fiber orientation in a disorganized scar.

Significance: These studies show that a thin wrap of electrospun silk, bonded over a tendon repair site, can have significant benefit to the repairing Achilles tendon. The silk wrap itself does provide some mechanical strength in holding the repair together at early times post-operatively and has a major impact in reducing the extent of post-surgical adhesions. Thus, a surgical scenario where the standard suture repair is augmented by the photobonded silk wrap (SR+ES/PTB) could provide optimal mechanical strength with reduced complication rates. Aligned ESA mats provide added mechanical strength and also a scaffold that organizes wound healing such that neo-collagen fibers are structurally similar to native tendon. This approach decreases complications due to suture and the extra strength provided by the ES mat should allow for earlier joint mobilization and a better functional outcome.

Publications and Abstracts:

1. Ni T, Senthil-Kumar P, Dubbin K, Aznar-Cervantes SD, Datta N, Randolph MA, Cenis JL, Rutledge GC, Kochevar IE, Redmond RW. A photoactivated nanofiber graft material for augmented Achilles tendon repair. *Lasers Surg Med*, Submitted April 2012.
2. Datta N, Lowery JL, Yao M, Wang Y, Ni T, Rutledge GC, Kochevar IE, Redmond RW. A photoactivated nanofiber material for tendon repair: Improved healing in a rat Achilles tendon model. *J Surg Res*, submitted May 2012.

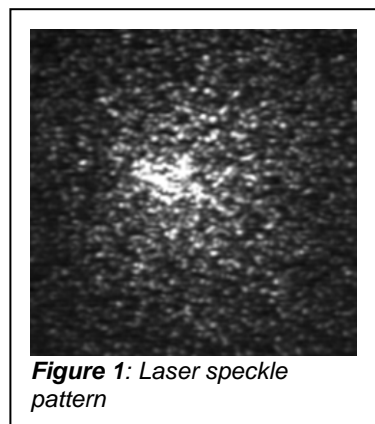
Patents filed for inventions funded: No new patents

Principal Investigator: Seemantini Nadkarni, PhD

Project Title: Optical evaluation of cartilage mechanical properties

Objective: *The goal of our research project is to investigate a new optical technology, Laser Speckle Imaging (LSI) to measure the mechanical properties of cartilage and evaluate cartilage degradation.* Osteoarthritis (OA) is the most common form of arthritis in military personnel. OA is characterized by the gradual degeneration of joint cartilage. Articular cartilage is the tissue covering the ends of the bones in diarthrodial joints and provides a lubricating surface for near-frictionless gliding of joints, while also absorbing and distributing mechanical loads onto the underlying bone. Cartilage is a viscoelastic material, composed of a viscous phase (65%-80% water) and a solid phase (extracellular matrix (ECM) proteins, proteoglycans (GAG)). A number of risk factors, including multiple molecular and morphological processes are cumulatively implicated in the progression of cartilage degeneration in OA. Compelling evidence points to the role of matrix metalloproteinases (MMP) that break down ECM proteins and expedite loss of GAG, resulting in changes in cartilage viscoelasticity. Progressive degeneration further compromises cartilage mechanical function, ultimately wearing the cartilage surface to the bone causing poor joint motion and severe pain. If early changes in cartilage viscoelasticity are detected, patients can be better stratified for therapies using disease modifying OA drugs (DMOAD) to reduce the rate of disease progression. There is a vital need to develop and translate new technologies for *in vivo* use that can detect early stages of OA and monitor small changes in cartilage viscoelasticity to evaluate response to therapy. While arthroscopy facilitates diagnosis of advanced OA, early stages present with nearly normal appearing cartilage on gross examination. We have developed a new optical imaging technology, LSI, that measures intrinsic Brownian motions of endogenous microscopic particles to provide measurements that are intimately linked with the micro-mechanical behavior of tissue. In the current project, we have validated the efficacy of the LSI technology in assessing cartilage degeneration in OA, with the long term goal of translating this technology for OA evaluation in patients.

Approach: LSI is a technique we have developed which offers the unique capability to provide measurements related to tissue mechanical properties. Laser speckle (Fig. 1) is a granular pattern formed by the interference of coherent laser light scattered from tissue. The intensity fluctuations of the speckle pattern are dynamically modulated by Brownian motion of endogenous microscopic particles within tissue, which is in turn governed by the viscoelastic properties of tissue. In the current proposal, we investigate the application of the LSI technology for measuring cartilage mechanical properties. Our hypothesis is that the rate of speckle intensity fluctuations, given by the speckle decorrelation time constant, τ , provides an invaluable metric to characterize cartilage mechanical properties in patients and monitor cartilage degeneration related to OA. In this project we have evaluated the validity of the LSI technique using engineered collagen scaffolds



and swine articular cartilage samples by comparing LSI measurements of time constant, τ , with conventional mechanical testing measurements of viscoelastic moduli. We have also conducted a study on excised human knee joints to correlate LSI measurements with changes in joint pathology using qualitative and quantitative Histopathological metrics.

Accomplishments:

1. LSI instrumentation: An optical system was fabricated to conduct LSI on cartilage samples. Light from a laser diode source (690 nm, 5 mW) was coupled into an optical fiber. The beam was expanded by 5:1, reflected off a mirror and focused to a 50 μ m diameter spot on the surface of the cartilage sample. A computer-controlled motorized stage was incorporated to scan the sample and a high-speed CMOS camera (Mikrotron MC 1310) used to acquire time varying speckle patterns.

2. Sample Preparation: The capability of LSI in evaluating tissue mechanical properties was tested in human cartilage samples. Cartilage samples (N=51) were obtained from human knees of 10 patients undergoing knee replacement surgeries at the MGH orthopedic surgery unit.

3. LSI data analysis: The LSI instrument was used to acquire time-varying speckle images at ~1kHz frame rate for a duration of 1s at each imaging site on the samples. The normalized 2D cross-correlation of the first speckle image with each image in the time-varying series was computed and the maximum value of normalized cross-correlation determined to obtain the speckle decorrelation curve, $g_2(t)$, for each sample. The rate of speckle decorrelation, given by the time constant τ , was measured by exponential fitting of the $g_2(t)$ curve. In human knee cartilage samples, based on %SO staining and additional morphometric parameters, a standardized modified Mankin scale (MMS) (score range from 0 to 10) was used to score the degree of cartilage degeneration, with score 0 corresponding to normal cartilage and score 10 corresponding to severe OA.

4. Key Results: Figure 2 shows an example of speckle decorrelation curves obtained from three cartilage samples with the corresponding saffranin-O stained sections. In (A), the curve exhibited a rapid rate of intensity decorrelation in the severe OA case (D) as compared with the normal (B) and mild OA (C) cartilage sites. Correspondingly, exponential fitting of the $g_2(t)$ curves yielded a lower time constants in the severe OA case

($\tau = 475$ ms) compared with the normal ($\tau = 964$ ms in B) and mild OA sites ($\tau = 783$ ms in C). B,

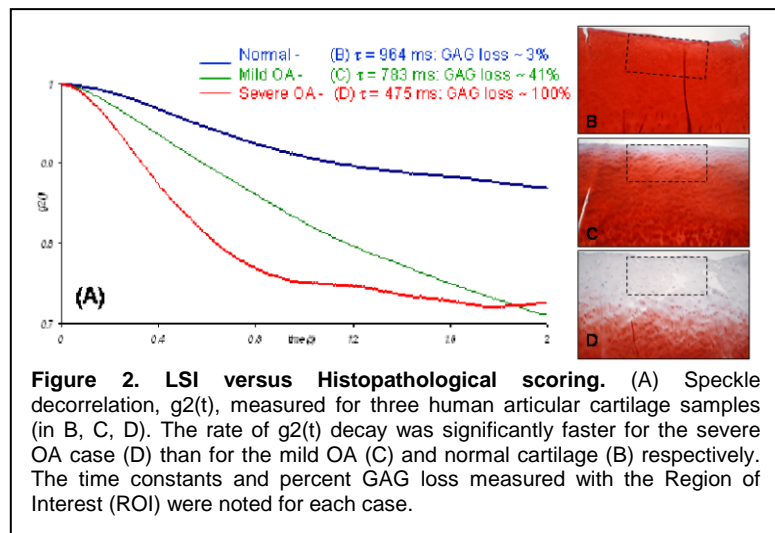


Figure 2. LSI versus Histopathological scoring. (A) Speckle decorrelation, $g_2(t)$, measured for three human articular cartilage samples (in B, C, D). The rate of $g_2(t)$ decay was significantly faster for the severe OA case (D) than for the mild OA (C) and normal cartilage (B) respectively. The time constants and percent GAG loss measured with the Region of Interest (ROI) were noted for each case.

C and D represent the progression towards OA, as seen in the successive loss of red %SO staining which measures GAG content. Image B (normal cartilage) had the highest intensity of red staining, followed by C (mild OA) which had mostly red staining accompanied by no staining on the tangential layer. D which corresponded to severe OA tissue was devoid of red staining within our ROI. The percent GAG loss was lowest in B (3 %), moderate in C (41 %) and highest in D (100 %). The decay of the $g_2(t)$ curves was consistent with the loss of staining. In (A), the $g_2(t)$ curve with the most rapid decay (red) corresponded to complete loss of staining in D while the curve with the slowest decay in $g_2(t)$ values (blue) was associated with no loss of staining (B). The $g_2(t)$ curve between normal and severe OA (green) showed moderate loss in staining.

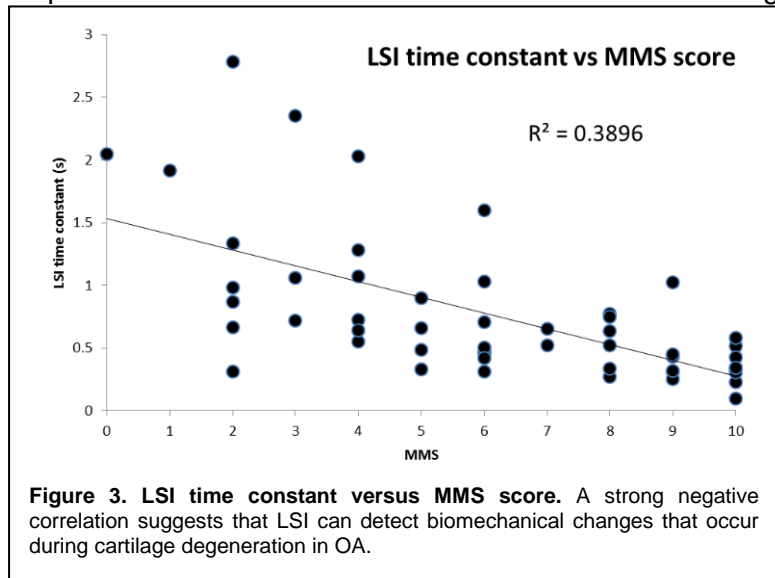


Figure 3. LSI time constant versus MMS score. A strong negative correlation suggests that LSI can detect biomechanical changes that occur during cartilage degeneration in OA.

As cartilage degrades, LSI rate of decay increased while τ values decreased. In addition, the intensity of %SO decreased and resulted in an increase in percent GAG loss— τ appeared to correlate with cartilage degeneration.

Figure 3 summarizes the data obtained from our human experiments where time constant τ , versus MMS scores (Fig. 5). A significant negative correlation ($R = -0.62$, $p < 0.01$) is observed between time constant τ and MMS score. These results suggest that LSI can detect changes in GAG content that occurs during cartilage degeneration in OA.

Significance: Based on the unique capabilities of LSI, and the promising results obtained during the project duration, we anticipate that this technology will provide a powerful tool for OA evaluation. We expect that the LSI time constant, τ , will provide a key metric that is closely related to cartilage mechanical properties and OA pathology. LSI is highly sensitive to the intrinsic Brownian motions of microscopic particles in tissue providing measurements that are closely related with small alterations in the micro-mechanical behavior of tissue. The current results show that this unique property of LSI will likely facilitate the detection of early OA changes, while also enabling the monitoring of OA response to therapy. LSI can be conducted using miniature optical fiber bundles⁴ and gradient index (GRIN) micro-lenses, potentially facilitating minimally invasive imaging in patients via needle based probes. We anticipate the LSI technology for cartilage evaluation will be highly relevant towards efforts in the development and discovery of new products for the treatment of OA. LSI has the unique potential to provide a highly sensitive tool for (i) identifying asymptomatic patients with early OA changes for therapy, and (ii) evaluating the effects of DMOAD therapies in altering cartilage mechanical function in OA. While the early detection and subsequent treatment of patients with OA can significantly improve patient quality of life, there is currently no technique that can identify and

monitor early OA onset and cartilage mechanical function in patients. We anticipate that the LSI technology will play a key role in meeting this vital clinical need.

Publications and Abstracts:

1. Evaluating the viscoelastic properties of tissue from laser speckle fluctuations. Hajjarian Z, Nadkarni SK. Sci Rep. 2012;2:316. Epub 2012
2. Measurement of bulk mechanical properties of tissue using laser speckle rheology. Hajjarian Z, Nadkarni SK. Conf Proc IEEE Eng Med Biol Soc. 2011;2011:5746-8.
3. Laser speckle Imaging for the mechanical evaluation of cartilage (Masters Thesis by Winnie Ong, Bon University) Project mentor: Nadkarni SK

Patents filed: none